COUPLING OF A TRAJECTORY OPTIMISATION STRATEGY TO LOCAL OPTIMAL SETPOINTS FOR ELECTRIC AIRCRAFT

H. Spark*, Y. Gazmawe* and F. J. Silvestre*

* Technische Universität Berlin (TUB), Department of Flight Mechanics, Flight Control and Aeroelasticity, Marchstrasse 12, 10587, Berlin, Deutschland.

Abstract

The task to extend the range of electric-powered aircraft is becoming increasingly important for manufacturers as well as for the general operation, leading to an increased importance of the trajectory optimisation field. A trajectory for a full flight mission can be optimised and generated by means of non-real-time calculations. This global trajectory optimisation relies strongly on weather forecast data. It consequently differs from the reality in its prediction of the energy expenditure, where actual environmental conditions as horizontal and vertical wind differ from the forecast. Therefore, in this present work, a local optimisation is used additionally. This local optimisation improves the efficiency in terms of range using measurements and information of local wind conditions. The main task of the local optimisation is to use the local wind data to set the optimal speed to fly continuously. Additionally, an optimal climb angle is determined in climb phases. For a global system that uses predicted wind and aircraft performance to generate a trajectory for a full flight mission and the local optimisation to be combined, the global and local systems must work in a clear procedure. This paper describes possible solutions to this problem and investigates the achieved energy reduction using the combined setup. The global optimisation procedure is based on dynamic programming. A reduced-order flight mechanical model for the simulation of aircraft capabilities and energy consumption based on forecast data is introduced. Generating an offline-database of the aircraft performance with this model, only feasible trajectories are determined. Furthermore, the calculation time of the optimisation is predictable, in contrast to solver-based optimisation procedures. For the local optimisation, a method to update setpoints to adapt to local measured wind distributions in real-time is described. An automatic flight control system is able to track those setpoints. Nonlinear simulation results show that the achievable energy savings in a test mission using the combined optimisation are significant.

Keywords

Electric Flight, Trajectory Optimisation, Guidance, TECS, Flight Dynamics Simulation

1. INTRODUCTION

Battery powered electric aircraft are challenged by weight restrictions due to manufacturers performance considerations or to comply with certification levels where aircraft weight is a major criterion. The low specific energy of batteries limits the available energy and range of such aircraft. Therefore battery-powered aircraft need to use the available energy as efficient as possible, focussing even more on range performance than on reducing travel time.

An electric glider configuration with a retractable propeller has two different configurations, one for climbing flight with extended propeller and one for gliding flight with a retracted propeller. In case the most efficient flight condition of the aircraft, aerodynamically seen, and the most efficient condition of the powertrain diverge, a flight tactic that oscillates between gliding and climbing flight is mostly efficient. This generally happens since there is an additional drag with extended propeller in non-gliding configuration in comparison to a clean configuration. For a fuel-powered glider this causality is described in Ref. [1]. Similarly, for a battery-powered electric glider with retractable propeller, the optimal flight also can consist of alternating segments of climbing and gliding flight. The result is highly dependent on the modelling of the powertrain and how its optimal setpoint diverges from the one of optimal clean-configuration glide. As shown by Settele [2], for an electric ultralight aircraft, optimised trajectories can be close to horizontal flight as the rate-capacity effect (also named Peukert effect) makes steep climbs at high power settings uneconomic. Reference [2] also uses performance indicators for electric flight range evaluation, the goal for all segments of flight is to maximise the range, i.e. minimise the charge drawn from battery for a specific distance in direction of a goal.

Dynamic Programming (DP) has successfully been applied to aircraft trajectory trajectory optimisation. Using linear flight path segments, Harada et al. [3] employed the BADA consumption model to generate fuel efficient trajectories. Oettershagen et al. [4] extended a DP algorithm to include weather data and a battery state of charge (SoC) parameter in the optimisation procedure. Ahmed et al. [5] improved further the algorithm applying

doi: 10.25967/610281

a modified dynamic programming approach that reduces the search space and numeric complexity of the problem. The latter has been selected in this work as basis for the global optimisation algorithm.
For locations in Germany, the ICON D2 weather forecast [6] predicts the 3D wind conditions for a grid of latitudes, longitudes and altitudes. As the latitude/longitude grid is in the scale of kilometers and the time resolution is one hour, this model does not include local wind effects as thermal updrafts. The dynamic programming method in this work uses this forecast data, the elevation profile of Germany as well as data of the flight performance of the used aircraft model. The trajectory generated with dynamic programming thus does solely adapt to a forecast condition.
Adaptions to local wind conditions are known in gliding flight, following MacCready rule for the minimum flight time. The best glide range is determined by the aircraft's glide polar. In the evaluation of the polar, local wind conditions can be incorporated [7] [8].
For battery powered electric aircraft, the best climb setpoint can be determined by evaluation of the state of charge change needed to climb to a specific altitude. This altitude can then be glided off, resulting in a sawtooth profile of alternating climb and glide segments. Adding up the horizontal distance in climb and glide and referencing it to the battery current draw in climb, the state of charge per range can be calculated. The use of this indicator for a climb performance is described in Ref. [2].
In the following, a performance model of a battery-powered electric aircraft with retractable propeller is introduced. This model is used in a dynamic-programming-based global trajectory planner to derive an a priori flight plan. Locally, the best-range speed-to-fly and the best-range climb performance are calculated online and serve to update the planner results. A safe distance to terrain must be maintained and the maximum airspace altitude must not be exceeded. Thus, an interaction of the online results and the planned altitude profile is described, such that the flown altitude profile resembles the planned altitude profile while allowing to adapt to the local wind conditions. The combined optimisation procedure has been applied to wind-less, adverse 2D- and 3D-wind conditions. Overall, nonlinear simulation results point to a considerable improvement in range performance.

2. MODELLING AND OPTIMISATION

In this section, the methods to model the flight performance of an electric motor glider and to optimise its trajectory in the longitudinal plane are described.

2.1. BATTERY AND EFFICIENCY MODELS

A reduced-order flight mechanical model is used for the simulation of aircraft capabilities and energy consumption in the trajectory optimisation. The results will be tested in a 6-DOF nonlinear simulation environment with precise table data for the powertrain performance. For the trajectory optimisation, the efficiency map of the entire electric propulsion system (propeller, motor and inverter) is modelled as a polynomial function fit of over true airspeed $VTAS$ and relative power setting δP $[0-1]$ with zero indicating no power draw from the battery and one being the maximum continuous power draw allowed. The fit is generated based on trim data of the nonlinear model. It is shown in Fig. 1. The battery is assumed to be 90 percent charged, as it represents a condition after an initial climb phase to minimal airspace altitude. The flight altitude showed a minor influence on overall powertrain efficiency (< 0.5 percent) and is neglected in the powertrain efficiency model but included in the reduced-order aerodynamic model.

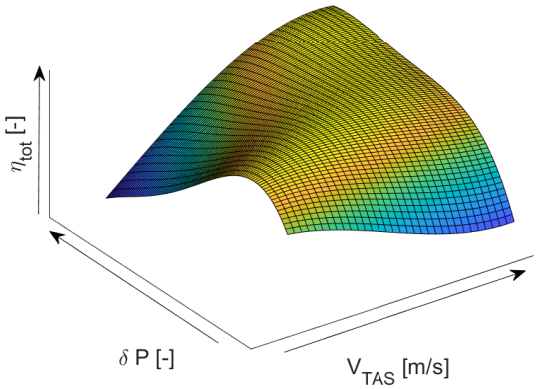

FIG 1. Powertrain efficiency map

It can be noted that, from the powertrain efficiency perspective only, a flight at high speed and maximum power setting is most suitable, whereas a flight at maximum power setting and low speed shows a considerable loss of efficiency due to unfavourable propeller flow conditions with the currently used fixed-pitch propeller.
Coupled to the powertrain efficiency model, a polynomial battery model determines the state of charge (SoC) difference for every simulation time step and calculates the effect of the discharge rate (Peukert effect) on the change of SoC. Based on a total energy control system (TECS) flight path angle and airspeed control for the reduced-order model, the thrust T and flight path angle (FPA) are used to determine the aircraft state in the next time step, see Fig. 2. Besides the powertrain efficiency model, the used set of equations of motion to model the performance of the electric glider include wind in all three axes and a quadratic drag polar.

2.2. GLOBAL OPTIMISATION AND FLIGHT PLAN DEFINITION

The global optimisation algorithm used to define the a priori flight plan employs a modified dynamic programming approach based on Bellman's principle of optimality [9] which states that individual parts of an optimal solution must also be optimal solutions to the problem at hand. Using this principle, the trajectory optimisation problem of minimal energy consumption at the target is

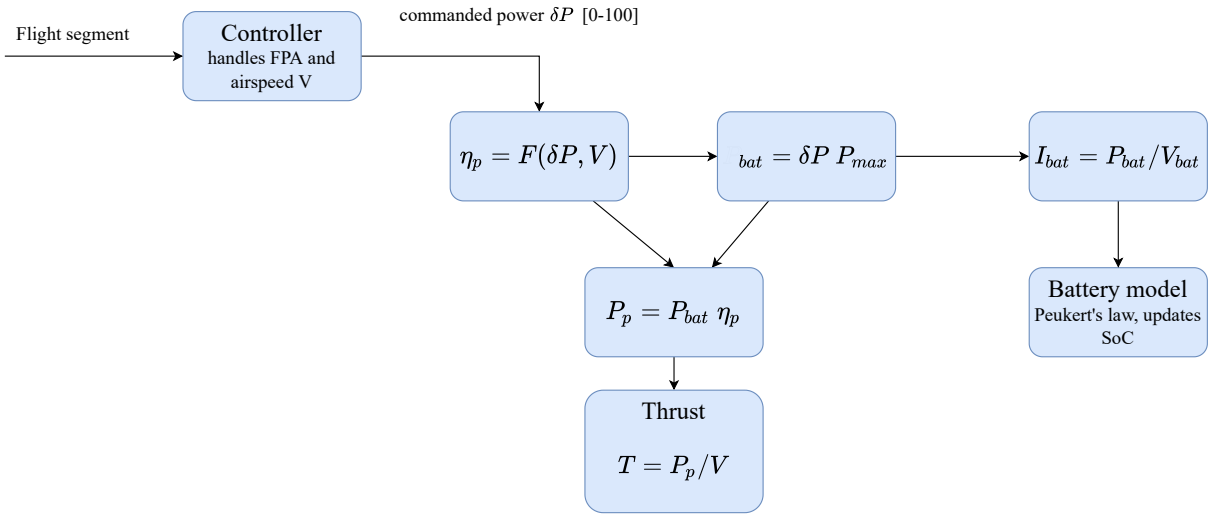

FIG 2. Efficiency modelling

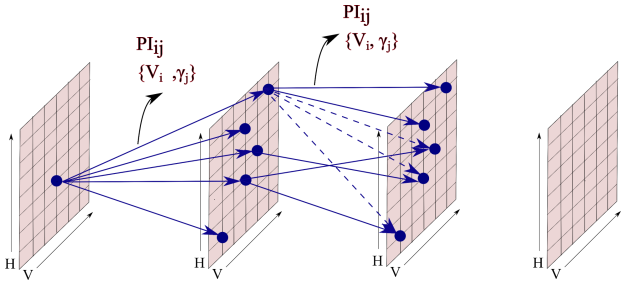

FIG 3. Speed and Altitude Grids in DP

split into subproblems that also are solved for energy-optimal solutions.

In a button-up approach, memoised results for recurring subproblems are used. This way, the computational effort of the algorithm is reduced. The subproblems are flights over a distance of 10 kilometers. The flights are varying the aircraft states of altitude and speed from beginning of the 10 kilometer flight to the end. The changes of altitude Δh and speed ΔV are defined by a grid of possible altitudes and speeds as shown in Fig. 3.

Transitioning from one grid state to another is done by controlling the 3-DOF optimisation model. Here, a total energy control system (TECS) is used to control the flight path angle and the airspeed. Thus, the same controller can be used for generating the dynamic programming performance database and for flying the 6-DOF aircraft in nonlinear simulation. The TECS controller is described in Ref. [10]. The 3-DOF simulation model for the optimisation uses the aircraft performance model of Sec. 2. The TECS controls the grid's altitude steps Δh with a fixed flight path angle γ and accelerates/decelerates according to the grid's speed changes ΔV. Thus, the energy needed for accelerations and flight path angle changes is included in the performance data that the dynamic programming approach uses. The flight dynamics model includes wind effects and a battery model that simulates the rate-capacity effect. A performance index (PI) of consumed battery energy per distance towards the target (see Eq. 1) is allocated to all unique transitions between altitudes and speeds in the grid.

$$PI = \frac{\Delta E}{\Delta x} \tag{1}$$

Using simulations with different starting altitudes and 3D wind conditions, the PI further includes the effects of the initial altitude and initial speed of the 10 km segment and the 3D wind condition. Some transitions are not feasible to fly the ten kilometer distances with the TECS controller, i.e. flying with an airspeed of 25 m/s with a headwind of 30 m/s. Infeasible transitions are automatically sorted out by evaluating the airspeed towards the goal in a steady state pre-trim. For trimmable conditions, the trim of angle of attack and power setting is used as initial condition and the flight of the 10 km segment is simulated. The flight is then evaluated if it reached the target altitude (can hold the flight path angle) and if the aircraft is able to accelerate to the target velocity. This reachability is saved in a reachability database. For each combination of starting conditions and inputs γ and ΔV, the corresponding PI is saved in a dedicated database. Based on this data sets of performance and reachability, the dynamic programming (DP) algorithm is evaluated for the energy optimal trajectory from the current location to the target location. The procedure is shown in Fig. 4. The algorithm outputs the optimal state trajectory of altitudes and airspeeds as well as the control value for the flight path angle.

The optimised trajectories are formatted to flight plans. A flight plan holds the information of waypoint (WP) latitude ϕ, longitude λ, WGS84 altitude as position information as well as the corresponding calibrated airspeed and

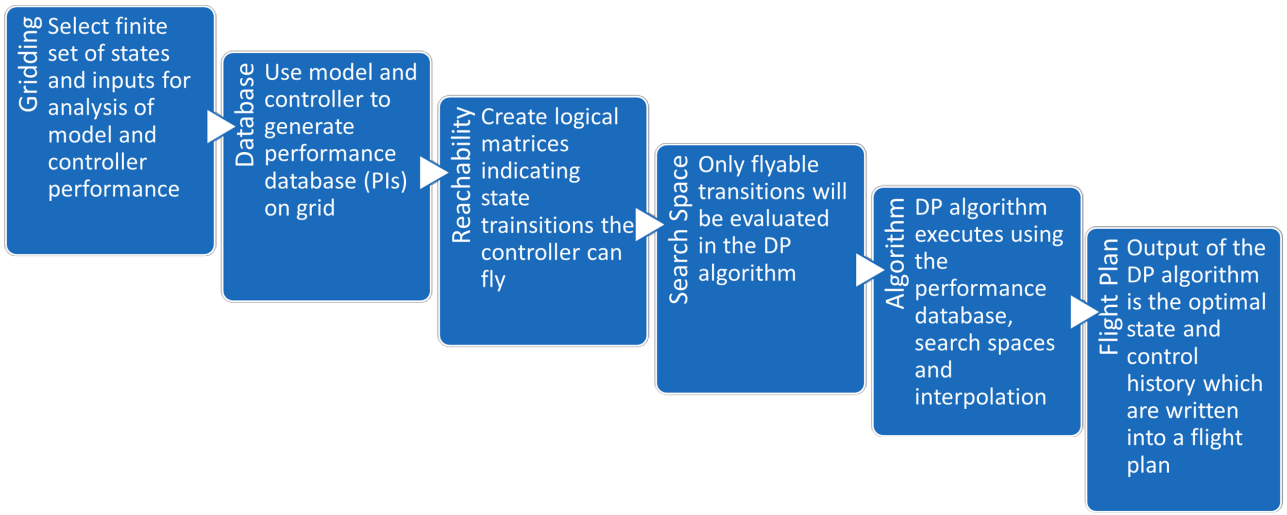

FIG 4. Dynamic Programming algorithm workflow

flight path angle as approaching conditions to the corresponding WP. Additionally, the optimised flight plans are evaluated and categorised according to the flight profile. If the flight plan solely holds climb and descend segments, the flight is categorised as sawtooth flight. Other options are horizontal and trapezoid profiles. The categorisation is added to the flight plan. For the sawtooth case, an interaction of the planner generated global trajectories and local optima is described in Sec. 2.4.

The planner software is programmed to run as an executable on an electronic flight bag (EFB). The planner communicates with the flight control computer. The flight control computer informs the planner tool of the current coordinates, altitude and speed as well as target location. The planner tool loads data packages of the elevation profile in Germany, the weather forecast and an aircraft performance database. The planner tool uses those data to generate energy-optimised trajectories from the current location towards the target.

2.3. LOCAL-WIND-OPTIMAL ADAPTIONS ON THE FLIGHT PROFILE

The adaptions to optimise range control the flight path angle, relative power setting and calibrated airspeed based on local wind conditions.

The wind-optimal settings are calculated separately for climbing and gliding flight.

For climb segments a module sets a pair of airspeed and flight path angle based on battery current draw. This climb reference is based on an electric aircraft climb flight performance index for sawtooth profiles as derived in Ref. [2]. This performance index is based on the assumption that by flying positive climb angles γ, gained altitude can glided off with the glide ratio E. Also, using small angle approximations and the relation $\dot{SoC} = \frac{I_{bat}}{C_{bat}}$ are used. The fixed battery capacity C_{bat} enables to use the battery current I_{bat} as indicator of battery energy draw per speed towards the target.

$$PI(climb) = max\big((1+\gamma E)\,\frac{V_{grnd,cl}}{I_{bat,cl}}\big) \tag{2}$$

In the climb performance index in Eq. 2, the ground speed in climb $V_{grnd,cl}$ and the battery current in climb $I_{bat,cl}$ which is a function of the motor power setting are used to calculate a performance index for the climb segment. Using the performance index, the best combination of flight path angle (FPA) γ, airspeed and relative power setting is selected as input to the aircraft controller. The optimal combinations are derived for several wind conditions, resulting in a table lookup of flight speeds for different wind conditions as in Ref. [11]. Local measurements of the wind conditions are used to index this offline-generated lookup in flight.

In gliding flight, speed to fly theory based on the aircraft's lift and drag polar with retracted motor is used to determine the calibrated airspeed. While gliding, altitude is not controlled but a result of flying the gliding speed. In glide segments, the best glide ratio speed can be calculated using a quadratic aircraft glide polar representation, see Ref. [8]. Including a horizontal wind component u_w, Depenbusch et. al. [7] give an algebraic approximation of the reference speed during gliding that additionally to the vertical wind component w_w also includes the contribution of horizontal wind from the front (positive u_w) or back of the aircraft to the glide polar based speed-to-fly rule in Eq. 3.

$$V_{ref,gl} = \frac{a\ u_w - \sqrt{a(a\ u_w^2 + b\ u_w + c - w_w - w_{cl})}}{a} \tag{3}$$

Herein, the parameters a, b and c are given by a quadratic fit of the aircraft's sink rate over the true airspeed. Using this rule in Eq. 3 results in the current vertical wind w_w and the current longitudinal wind being taken into consideration for the calculation of the airspeed that maximises range in gliding flight.

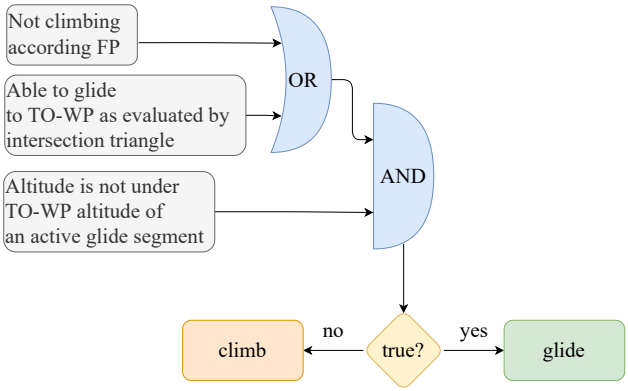

FIG 5. Interaction with sawtooth type flight plan

This formula provides real-time computation of the optimum glide speed in local wind conditions but this formulation does not converge for strong vertical winds as the square root turns complex when updraft exceeds the aircraft sink polar in Eq. 3. Thus, herein the speed-to-fly in gliding flight is calculated by an interval search algorithm giving similar results but avoiding problems in the evaluation of strong thermals.

2.4. COUPLING OF NAVIGATION AND WIND-OPTIMAL GUIDANCE

The flight control functions have the flight path angle, relative power setting and the airspeed as degrees of freedom for adaption to local wind conditions. This adaption takes place in the wind-module at the guidance hierarchy level, one level below the navigation level.
As the flight plan, generated by the global planner, also prescribes flight path angles and airspeeds that are based on weather forecast data, an interaction of the flight controller and the planner takes place.
If the flight plan is marked as type sawtooth by the EFB planner, the guidance controller adapts to deviations from the altitude profile in the flight plan.
Deviations from the flight plan can arise if the the weather forecast or the aircraft performance model are not similar to the actual conditions or if locally strong vertical wind is encountered. The module adapts to deviations from the flight plan by selecting either climbing or gliding flight, deviations from the waypoint-defined flight path angles are allowed as long as safe altitude above terrain and the airspace altitudes are respected.
The FPA information is part of the waypoint data for the next waypoint that is closest to the current aircraft position, which is visible to the guidance controller as the active waypoint.
Following conditions are accounted for:

- **climb according to FP:** Aircraft is below maximum altitude of airspace and FPA read from flight plan is positive.
- **climb overshoot of FP altitude:** The current altitude exceeds the top of climb (TOC) altitude based on the flight plan.
- **climb undershoot of FP altitude:** The current altitude is below the TOC altitude specified in the flight plan as the aircraft reaches the active WP position.

TAB 1. Guidance actions for FP deviations

condition	action
climb overshoot	intersection triangle
climb undershoot	early glide
glide undershoot	early climb
glide overshoot	climb according to FP

- **glide overshoot:** The current altitude is above the end of descend (EOD) altitude specified in the flight plan as the aircraft reaches the active WP position.
- **glide undershoot:** The current altitude is below the EOD altitude specified in the flight plan.

For these conditions, actions are defined. The actions follow the principle 'if in doubt, climb out'. Thus, the controller defaults to climbing flight and only allows gliding flight based on the logic shown in Fig. 5. For an overview of adaptions, see Fig. 6.
These adaptions allow climbing over the top of climb (TOC) altitude but not gliding below the end of descend (EOD) altitude. An intersection triangle method handles the transitions from climb to glide segments. It is based on the geometry shown in Fig. 7.
The triangle method activates the calculation of a climb to glide switch condition. The condition is met, if the current aircraft position allows to transition to the next glide path based on average glide performance excluding local wind effects. With the distance `distTO` to the active WP `WPTO`, the transition to the glide (index gl) phase is evaluated in climb (index cl) by calculating:

$$h_{trans} = -\tan(\gamma_{gl}) \cdot \texttt{distTO} + h(\texttt{WPTO}) \tag{4}$$

If the current altitude is over the transition altitude h_{trans}, gliding flight is activated.
The conditions of glide undershoot (when the aircraft is under the waypoint TO-altitude in glide segment) and a valid intersection triangle are only evaluated once per segment to avoid multiple retractions/extensions of the propeller in one segment of the flight plan.
The mapping between conditions and actions is summarised in Table 1. The condition of climb undershoot is resolved by changing to the glide segment as according to the flight plan. Synchronisation with the flight plan altitudes will be solved in the next glide segment.
Arriving at the destination, the interaction with the flight plan guarantees to be over the target altitude if the last flight segment is a glide segment.
Additionally, in gliding segments, the motor is retracted to reduce aerodynamic drag and the pitch is based on airspeed control. In contrast, for climbing segments the pitch is based on airspeed and flight path angle control.

2.5. NAVIGATION AND GUIDANCE LEVEL

Currently, the experimental setup employs a tablet computer as electronic flight bag, running the dynamic programming algorithm that calculates a new flight plan. The experimental setup uses a desktop computer for non-

WP Altitudes	
WP 1	600
WP 2	1350
WP 3	750
WP 4	1100
WP 5	700
WP 6	1400

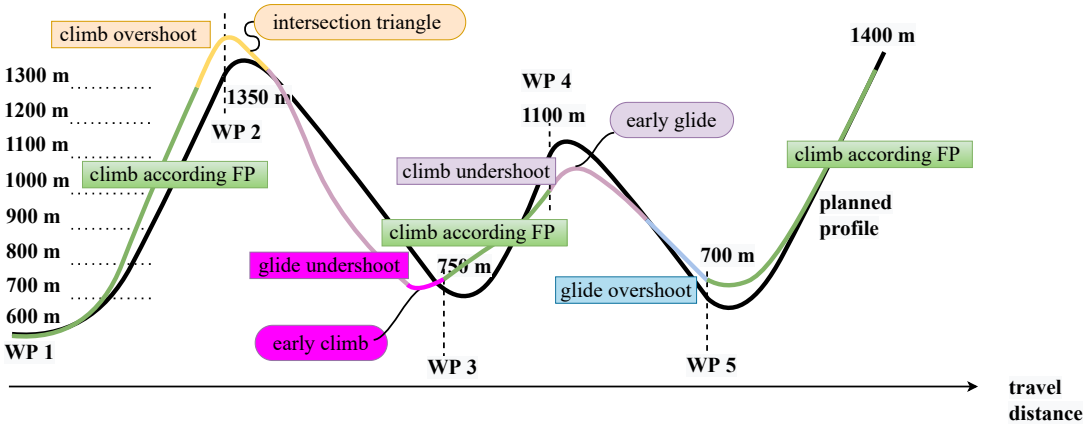

FIG 6. Interaction with sawtooth type flight plan

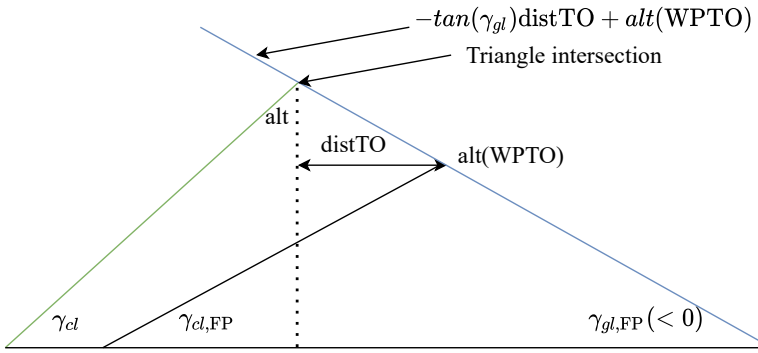

FIG 7. Intersection triangle definition

linear simulation of the electric glider aircraft coupled to a flight control function in a closed-loop simulation.
In the current state, the concept of operation leaves the tasks of aircraft start and landing to the pilot. After initial climb, the altitude range in the E-class aerospace in Germany is reached. It is defined by the altitude range of approx. 600 m above ground level (AGL) up to 2900 m. In this range, the autopilot (AP) can be safely activated by the pilot. In a vectoring (VEC) mode, the pilot enters directly flight path angle, ground track and flight speed. It can be seen as a pilot relief mode or a transition mode to a waypoint navigation (NAV) mode. The NAV mode is employing the local-global optimisation methods and thus uses the generated energy efficient flight plan.
In the following, the logic to trigger this optimisation is explained.

2.6. OPTIMISATION TRIGGER

The flight control software starts in VEC mode and tracks the set altitude or flight path angle and speed. Starting from this condition, the VEC mode can be a transition mode as a filed flight plan (FP) triggers the activation of the NAV mode, see Fig. 8. A flight plan is calculated by the EFB planner program. As the execution of the optimisation is fast, the planner tool can start its calculation based on the current position and velocity. Aside from triggering the calculation of an initial flight plan, the planner can be retriggered with the flight control software in NAV mode. Receiving new weather forecast data by a download can be a reason to retrigger the calculation of the flight plan and use the latest forecast for the flight plan optimisation. The flight plan calculation trigger logic is shown in Fig. 8.

3. PERFORMANCE ANALYSIS

The effects of the optimisation are investigated in a nonlinear simulation environment. This nonlinear simulation uses table data of battery and motor performance as well as of the aerodynamic. In contrast, the reduced order model in the planner tool uses polynomial representations of the powertrain and battery behavior for simulation speed. First, a windless simulation with a fixed altitude of 600 m and fixed airspeed of static best range speed is evaluated as a reference case. Then, a sawtooth profile is employed on the windless environment. Afterwards, a sawtooth profile as commanded by the flight plan is generated with wind information of the ICON D2 model described in Ref. [6]. The test gives output on the interaction of the guidance controller with the flight plan. Introducing a deterministic wind profile, lastly a flight with 3D wind is simulated and the benefit of the optimisation as well as the usability of the interaction of the guidance law with the flight plan is investigated. In each case, the mission starts at an altitude of 600 m with 100 percent state of charge. The performance analysis is done on a flight from Berlin to Hessen. Figure 9 shows the ground track and elevation profile for the flight. The evaluation starts at 600 m and ends at 1600 m such that the waypoint stay over 2000 ft above the terrain. Figure

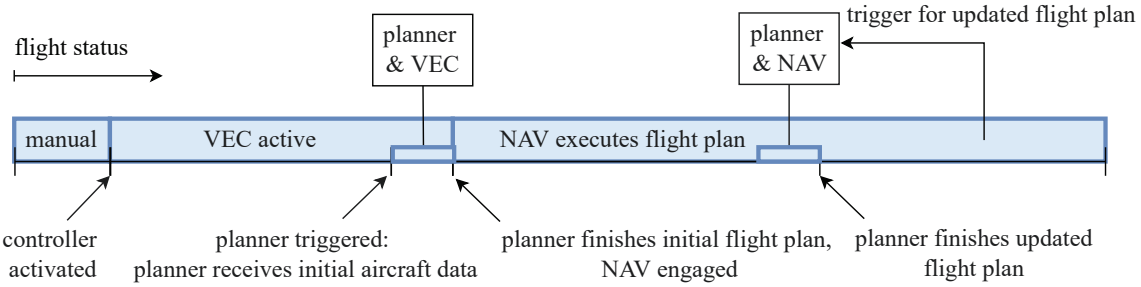

FIG 8. Trigger for flight plan calculation

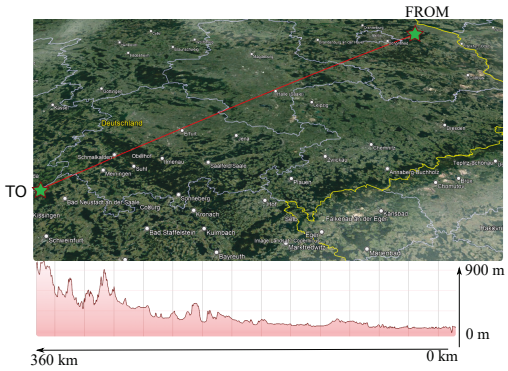

FIG 9. Flight and terrain profile

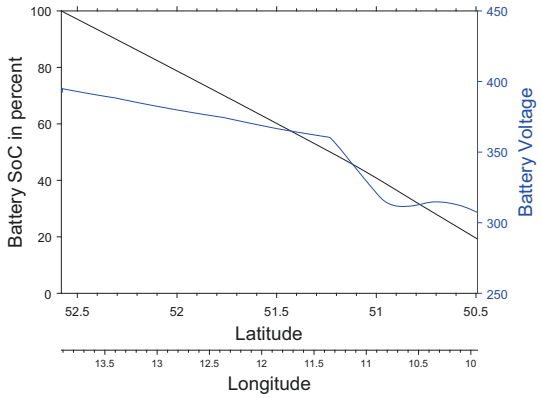

FIG 10. Battery parameters for level flight in wind-less environment

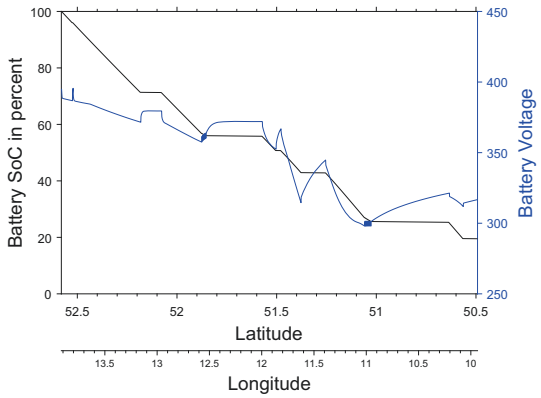

FIG 11. Battery parameters for sawtooth in wind-less environment

14 gives the static horizontal wind condition for different flight altitudes.

3.1. WIND-LESS MISSION

Without wind influence and with the start and target altitude at the same value, the elevation profile of the mission is neglected a horizontal comparison flight. For a level flight at 30 m/s and 600 m altitude, Fig. 10 shows the battery parameters over latitudes and longitudes of the flight. The following plots have been generated with the plotter tool of Ref. [12]. The remaining SoC at the target is $19,20$ percent. For comparison, the mission is flown with the sawtooth tactic using the flight plan generated by the dynamic programming approach and the local optimisation. This flight plan includes terrain avoidance. Figure 11 gives the battery parameters for the optimised flight. The SoC at the target is $19,51$ percent, indicating an advantage though the final altitude is 1000 m above the altitude of the horizontal comparison flight. The climb segments are characterised by voltage drops, in the glide segments the SoC is constant and the battery voltage recovers slowly towards values that are correlative to the respective SoC. The altitude and speed profiles of the level flight showed no indications of deviating the setpoints as wind is not engaged (not shown). The sawtooth profile uses airspeeds that are close to the level flight setpoint of 30 m/s as shown in Fig. 12. Minor airspeed peaks can be seen in the transitions from gliding flight to climbing flight, also as the propeller extension and retraction are currently modelled as being instantaneous transitions. The altitude profile as generated by the planner tool and the actual altitude profile are shown in Fig. 13. The actual profile is not the same as the planned profile but is synchronised by the triangle intersection method. The actual climb angle as evaluated by local optimisation is not as steep as the planned climb angle as can be seen in the second climb. This may be attributed to the use of different methods for the generation of the planner profile and the local optimisation. With different climb angles, an early glide condition transitions the aircraft to a glide and the planned altitude of the second climb is not reached. This results in reaching the end of descend altitude in the following descend too early, triggering an early climb. In the following climb, the aircraft is synchronised with the flight plan by the climb overshoot intersection triangle. However, the maximum airspace altitude of 2900 m is reached and a short

horizontal segment is thus included to not exceed the maximum altitude. The altitudes do not undershoot the TO-WP altitude specified by the planned profile. Those TO-WP altitudes are set by the planner and respect the distance to terrain for the whole flight segment, i.e. no terrain is closer than 2000 ft if the segment was flown with the TO-WP altitude throughout.

3.2. WIND INFLUENCE

The modelled wind consist of forecast dependant 3D static wind field and a measurement-based vertical wind profile. Both static wind and vertical wind profiles are position-dependent. Furthermore, the static wind is altitude-dependent. The weather forecast includes meteorologic effects e.g. the wind rotates in the planetary boundary layer (the bourdary layer expands up to over 1000 m as described by Ref. [6].) Figure 14 shows the northwards and eastwards wind at different altitude layers.

The vertical wind in the forecast data is negligible, as the forecast data resolution does not show thermal activity.

Figure 14 shows the wind rotation over the altitude as included in the used forecast data. The markers placed in Fig. 14 indicate the horizontal wind vector [zonal wind component U, meridional wind component V] and are attached to the 3000 m wind. The 3000 m wind rotates when comparing the marker position at the northwest side of the wind field and the marker position to the east. The horizontal wind is of low to medium intensity (around 8 m/s). The vertical wind is modelled as not altitude-dependent and shown in Fig. 15. It is taken from flight measurement data in Ref. [13].

3.3. OPTIMISED FLIGHT WITH HORIZONTAL WIND INFLUENCE

The dynamic programming algorithm on an electronic flight bag calculates the altitude and speed profile needed for the flight plan generation. Those calculations include the effect of the static horizontal wind. The output of the global optimisation is the planned trajectory in the flight plan. The planned trajectory is shown in Fig. 16. The flown altitude profile, as established by the interaction of local optimal flight and planner trajectory, is also indicated in Fig 16. The trajectory is lower than the one planned for the wind-less case as the wind direction turns unfavourable with increasing altitudes, see Fig. 14. The planned aircraft waypoint speed is close to 30 m/s most of the flight. The SoC and battery voltage development over the flight are given in Fig. 17.

The target is reached with $9,24$ percent SoC remaining and slightly over the target altitude.

There are twelve climb and also twelve glide segments for a total of 22 planned alternating climb and glide segments. The additional segments are introduced by the guidance actions for flight plan deviations i.e. to intercept the flight plan. The end of descend (EOD) altitudes as defined in the flight plan are not violated and a safe distance about 600 m over terrain is established. The fast planning time of the EFB flight plan generation tool allows to enter the optimised altitude profile shortly

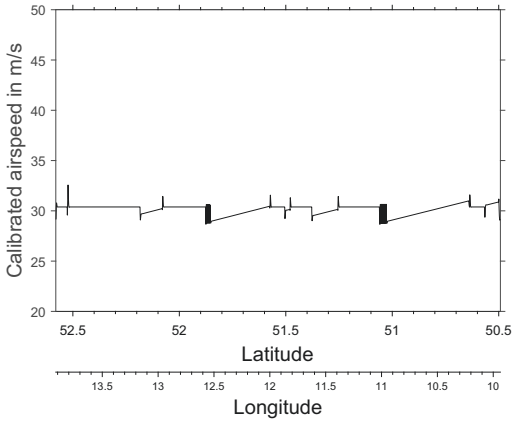

FIG 12. Airspeed profile for sawtooth in wind-less environment

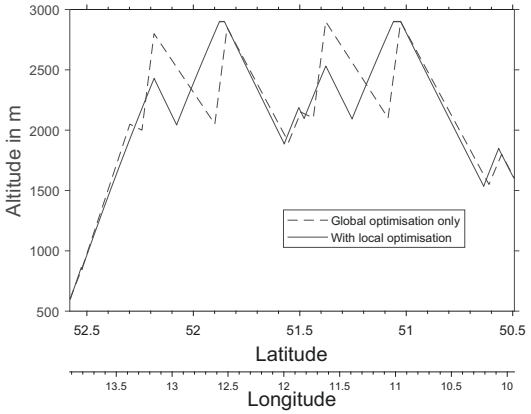

FIG 13. Altitude profile in wind-less environment

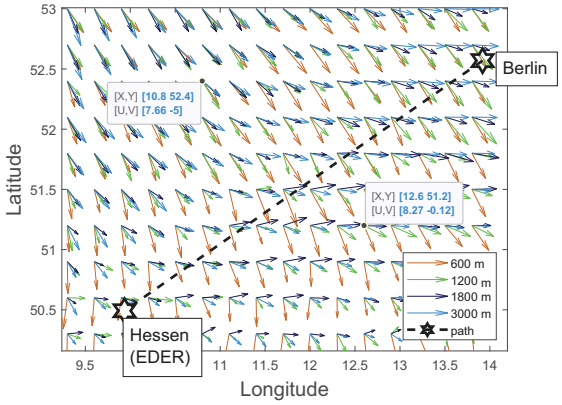

FIG 14. horizontal wind over the flight distance

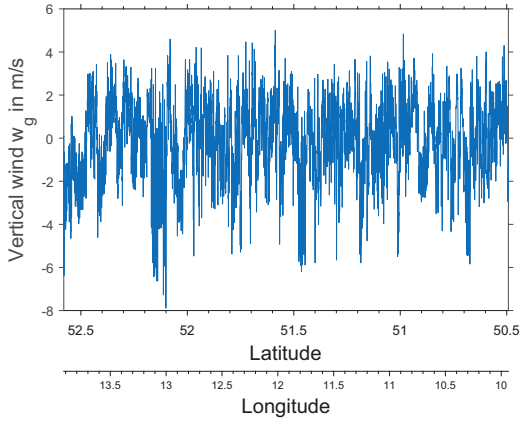

FIG 15. Vertical wind profile

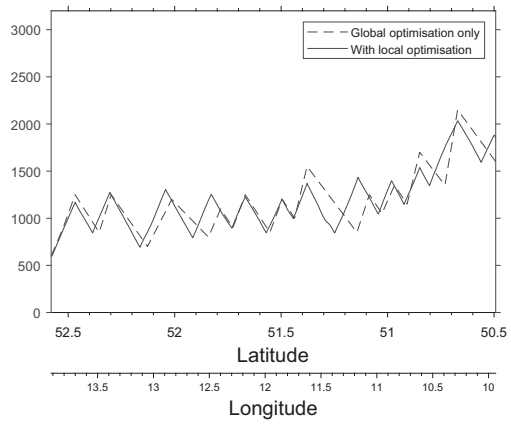

FIG 16. Sawtooth altitude profile with horizontal wind

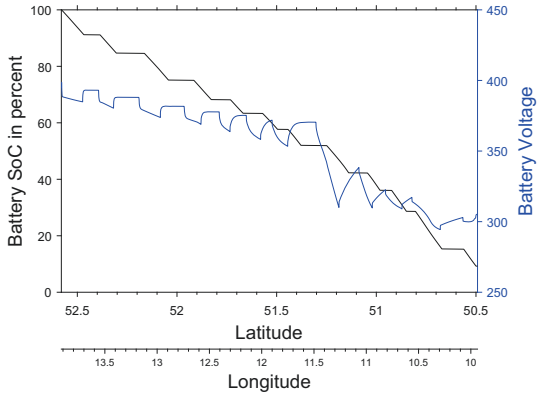

FIG 17. Battery parameters for optimised flight with horizontal wind

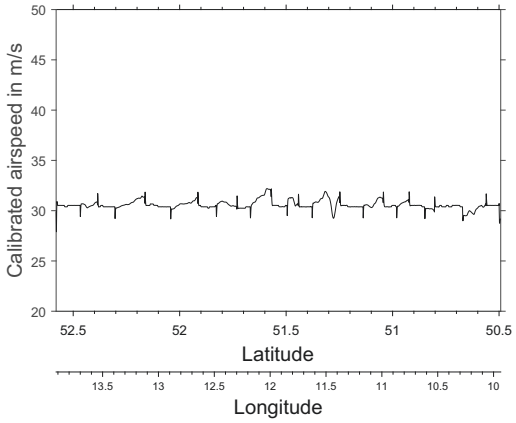

FIG 18. Flown airspeeds in nonlinear simulation for optimised flight with horizontal wind

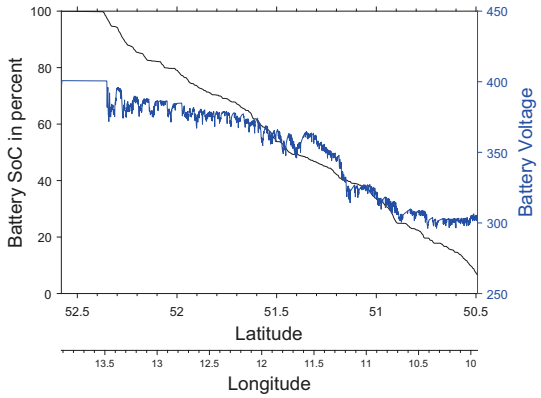

FIG 19. Battery parameters for level flight in 3D wind

after controller activation. The calibrated airspeed as controlled by the speed to fly adaptions in the guidance controller is shown in Fig. 18. The airspeeds are close to the wind-less optima of 30 m/s. Thus, the low to moderate horizontal winds did not lead to significant airspeed adaptions.

3.4. LEVEL FLIGHT WITH HORIZONTAL AND VERTICAL WIND INFLUENCE

In level flight at fixed calibrated airspeed setpoint of 30 m/s, with the inclusion of vertical wind (see Fig. 15) target latitude and longitude are reached, but at 600 m altitude. The battery is discharged to $6,61$ percent, the SoC development is shown in Fig. 19. This is $12,59$ percent worse than in the wind-less mission with level flight tactic. As a climb to 1600 m is consuming about ten percent of charge, the level flight approach may not be suitable for this mission.

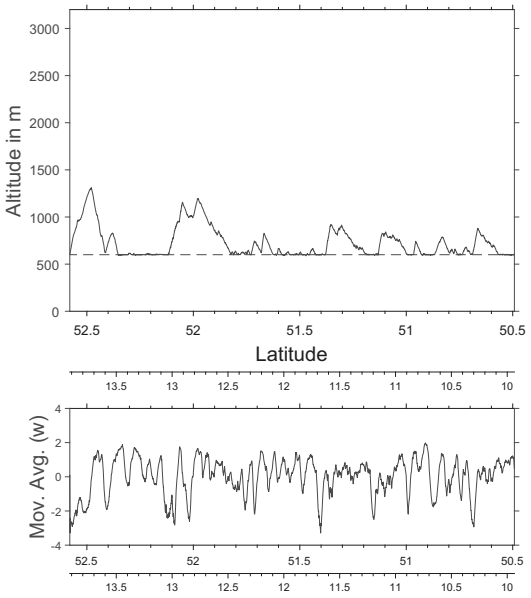

FIG 20. Altitude for level flight commanded at 600 m in 3D wind and moving average of vertical wind

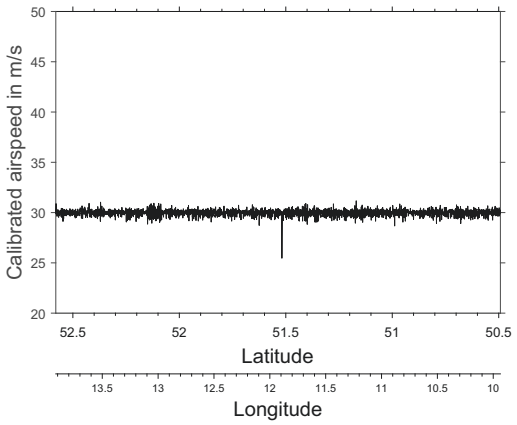

FIG 21. Airspeed for level flight in 3D wind with fixed target airspeed

As can be seen in the altitude profile in Fig. 20, strong updraft present in the vertical wind profile lead to unintended climbs up to 600 m over the reference altitude. This is due to the airspeed-hold at 30 m/s, as indicated by Fig. 21. If altitude was prioritised over airspeed, the airspeed would increase significantly to burn the excess energy, reducing the available range.

3.5. OPTIMISED FLIGHT WITH HORIZONTAL AND VERTICAL WIND INFLUENCE

The wind now strongly deviates from forecast in vertical axis with the mean of vertical wind close to zero. The local optimisation adapts to vertical wind, resulting in reduction of airspeed in updrafts and vice versa as shown in Fig. 22.
In glide segments, optimum speed is favoured over altitude accuracy when compared to the flight plan altitudes shown in Fig. 23.
With the strong vertical winds, the trajectory deviates from flight plan more than in the case without vertical wind shown in Fig. 16. As in the wind-less and horizonal wind cases, there is no undershoot of the end of descend (EOD) altitudes. The top of climb (TOC) altitudes as defined by the flight plan are exceeded, but the intersection method at the glide segments leads to a good capturing of the waypoint altitudes at the end of the glide phases. SoC and Voltage are shown in Fig. 24. The SoC at the target is $14,89$ percent. This SoC is $5,74$ percent higher than when compared to the mission with only horizontal wind. Additionally, it is $4,53$ percent worse than without wind, considering the horizontal wind is adversely influencing range. Thus, the vertical wind adaptions by the local speed to fly optimization increased the range significantly.

4. CONCLUSION

A global trajectory optimisation algorithm based on weather forecast, resulting in a sawtooth mode consisting of alternating climb and glide segments was coupled to a local wind optimisation that generates an updated reference. The setup prioritises the local wind-sensitive optima over the sawtooth waypoint list as generated by the global optimisation method. As global optimisation method, a dynamic programming approach was developed using a polynomial powertrain efficiency model and a battery model that includes the rate-capacity effect. It respects a safe distance to terrain and uses weather forecast data and not information of the local wind which strongly deviates in the vertical axis.
An interaction method was introduced that allows to exploit thermal updrafts by climbing over waypoint altitudes but protects from undershooting end of descend altitudes to protect against low flight heights (terrain). Using the waypoints generated by the planner and the sawtooth mode in a wind-less environment, the consumed battery energy was reduced while the planner reached a target altitude 1000 m above the target of a level comparison flight. Thus, for the simulated aircraft the saw-

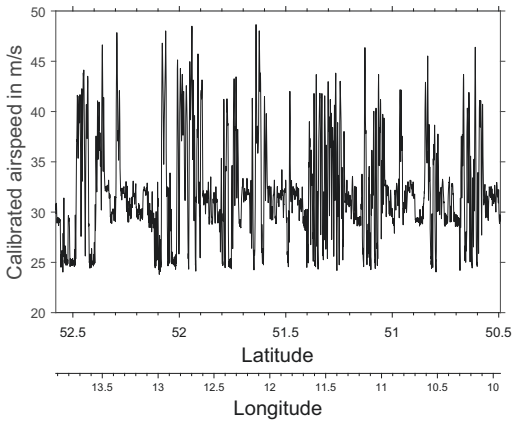

FIG 22. Calibrated airspeed for optimised flight in 3D wind

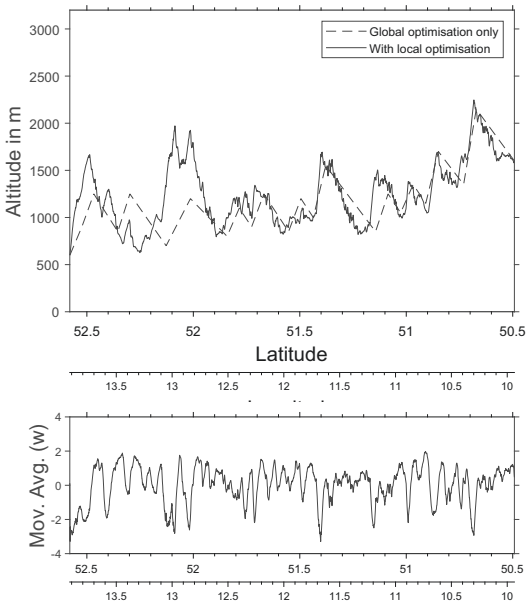

FIG 23. Altitude profile for optimised sawtooth flight and moving average of vertical wind

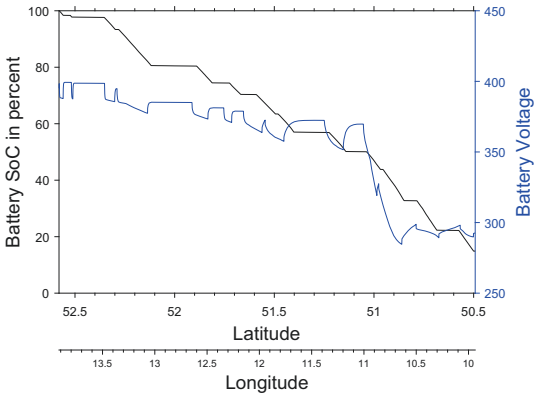

FIG 24. Battery parameters for optimised flight in 3D wind

tooth mode increased the range. Furthermore, a test case of a mission from Berlin to Hessen showed that the coupling between dynamic programming and local wind-sensitive optimisation was able to arrive at the target avoiding terrain in adverse wind conditions. The local optimisation was able to increase the range by exploiting vertical winds. The SoC increase by using the vertical wind was $5,74$ percent and the overall SoC decrease by the adverse 3D-wind was only $4,53$ percent while with level flight tactic and fixed airspeed, the SoC decrease through wind was $12,59$ percent. As a level flight tactic ended this mission at $6,61$ percent state of charge and 1000 m below the target altitude, the mission starting from 600 m and arriving at 1600 m may not be possible when using a horizontal flight tactic. With the coupled optimisation, the SoC at the target altitude of 1600 m was $14,89$ percent. Thus, this mission is only enabled by using optimisation.

To conclude, both elements of optimisating a sawtooth mode flight plan and adapting to local wind conditions are able to extend the range by decreasing energy consumption. A safe combination of both with fast flight plan generation and real-time local wind adaption is generated.

The framework introduced in this paper is able to recalculate the trajectory and rewrite the flight plan that the guidance controller uses. This can be very advantageous if updated wind information is available.

Contact address:

spark@tu-berlin.de

References

[1] G. Sachs, J. Lenz, and F. Holzapfel. Trajectory optimization for maximizing the range of powered sailplanes with retractable propeller. In *AIAA Guidance, Navigation, and Control Conference.*, volume 2009.

[2] F. Settele. *Strategien zur energieoptimalen Flugführung eines batterie-elektrisch angetriebenen Leichtflugzeuges*. 2021, Phd. Thesis, Technical University of Munich.

[3] A. Harada, H. Matsuda, and Y. Miyazawa. Dynamic programming trajectory optimization by piecewise linear approximation. In *AIAA Guidance, Navigation, and Control Conference*, Reston, Virginia, 2015. American Institute of Aeronautics and Astronautics. DOI: 10.2514/6.2015-1075.

[4] P. Oettershagen, J. Förster, L. Wirth, G. Hitz, R. Siegwart, and J. Ambühl. Meteorology-aware multi-goal path planning for large-scale inspection missions with solar-powered aircraft. *Journal of Aerospace Information Systems*, 16(10):390–408, 2019. DOI: 10.2514/1.I010635.

[5] K. Ahmed, K. Bousson, and M. d. F. Coelho. A Modified Dynamic Programming Approach for 4D Minimum Fuel and Emissions Trajectory Optimization. *Aerospace*, 8(5):135, 2021. DOI: 10.3390/aerospace8050135.

[6] D. Reinert, F. Pril, H. Frank et. al. DWD Database Reference for the Global and Regional ICON and ICON-EPS Version 2.2.1, 2023.

[7] N. T. Depenbusch, J. J. Bird, and J. W. Langelaan. The autosoar autonomous soaring aircraft, part 1: Autonomy algorithms. *Journal of Field Robotics*, 35(6):868–889, 2018. DOI: 10.1002/rob.21782.

[8] H. Reichmann. *Streckensegelflug*. Motorbuchverlag, Stuttgart, 2005. ISBN: 3613024799.

[9] R. Bellman. *Dynamic Programming*. Princeton University Press, 6 edition, 1957, 6.th Ed. 1972. ISBN: 0-691-07951-X.

[10] H. Spark, P. J. González Ramirez, C. Ruwisch, W. Meyer-Brügel, and F. J. Silvestre. Development and experimental testing of flight path control using total energy control and siso control loops. In *AIAA SCITECH 2023 Forum*, Reston, Virginia, 01232023. American Institute of Aeronautics and Astronautics. DOI: 10.2514/6.2023-0104.

[11] T. Mörsel. SERELA-APUS : Abschlussbericht : Project 2015-038, 2019. DOI: 10.2314/KXP:1667785524.

[12] R. Pawlowicz. plotmultix(varargin), MATLAB Central File Exchange, Retrieved July 17, 2023, https://www.mathworks.com/matlabcentral/fileexchange/65044-plotmultix-varargin.

[13] L. Hagemann and S. Auen. Segelflugaufzeichnung Bayreuth: Arcus T, 31.05.2023, https://www.weglide.org/flight/271585.